

# On the Leading Edge Cavitation In a Helico-centrifugal Pump : Experimental and Numerical Investigations

D Pierrat, L. Gros\*, A. Couzinet, G. Pintrand

Cetim, 74 route de la jonelière, BP 82617, 44326 Nantes Cedex 3 - FRANCE

Ph. Gyomlai

AREVA JSPM, 27 rue de l'industrie 59460 Jeumont - FRANCE

## ABSTRACT

This paper deals with the leading edge cavitation of the impeller of a single stage helico-centrifugal pump. In the one hand, in order to perform experimental investigations, a specific impeller with transparent shroud and a special casing with windows have been used as experimental test rig. The leading edge cavitation has been experimentally observed on the both sides of the impeller and the head drop measured for different operating conditions.

In the other hand, a CFD model for cavitation simulation has been investigated and compared to experimental results for 3 flowrates, ranging from 0.85  $Q_n$  to 1.25  $Q_n$ . The model uses a multiphase approach, based on a homogeneous model assumption. A truncated form of Rayleigh-Plesset equation is used as a source term for the inter-phase mass transfer. Comparisons between experimental and numerical results are presented and the cavitation figures are in a good agreement with the experimental ones for each flowrate.

## KEYWORDS

Cavitation, Helico-centrifugal pump, CFD computations, numerical modeling

## 1. INTRODUCTION

Cavitation phenomenon is still a limiting factor in the design of hydraulics turbomachines. When cavitation has enlarged, it is responsible for the noise and vibration generation, for the erosive damage with premature wear of the exposed surface, and for the loss of performance. Cavitation in turbomachines appears at operating conditions where the pressure locally drops to and below the vapour pressure.

CFD software has become essential to determine the set of operating conditions or modes that leads to cavitation. Such tools can be applied for two types of objectives. First, they are used for engineering and design purposes. The physical models are then relatively simple but assumptions are rather restrictive: indeed, they are based on a steady state approach and turbulent effects are most often modelled with the so-called eddy viscosity concept. Cavitation itself is modelled at a first order approximation of a vaporization model mainly based on the thermal and mechanical equilibrium assumption between liquid and vapor phases. Many works demonstrated that these models still give correct estimates of the loss efficiency and cavitation inception. Computation time is acceptable and compatible with industrial timeframes [2-4]; [5]; [10]; [11]; [13]; [15-18]; [26]; [27];[28].

The second approach, which will not be developed in this work, is more focused on the transient aspects of the flow structure and of cavitation [5]; [7]; [19]; [22]; [30]; [32].

\* Corresponding author: phone: +33 240 373 544, fax: +33 251 864 623, email: laurent.gros@cetim.fr

Most of recent works on the first approach concerns three-dimensional inducers [2-5]; [10]; [11]; [17], and in a lower proportion, centrifugal pumps [13]; [15]; [17]; [23]; [26].

We consider in this current work the appearance of cavitation phenomena on helico-centrifugal pump. Experimental investigations have been lead on CETIM's ridge and numerical prediction of this behaviour has been investigated around nominal point. The commercial CFD packages ANSYS-CFX has been used to run numerical studies. Results obtained are compared with experimental data such as Head, NPSH, efficiency and cavitation development on the blade. The cavitation model used is the default one implemented in these codes. It is based on the so-called VOF (Volume of Fluid) model. In order to simulate the liquid/vapour mass transfer, a mass source term in the volume fraction transport equation is derived from a first order approximation of the Rayleigh-Plesset equation [5]; [11].

Major restrictions for design studies are realisation costs and delays. Velocity-pressure coupling method is particularly efficient to solve non-cavitating flows for turbomachinery. It enables the use of relatively fine grids without reaching prohibitive calculation costs, especially for conditions getting far from nominal ones. Nevertheless, the use of a cavitation model makes the Navier-Stokes equations behave in a highly non-linearly mode; this removes the possibility of working on such fine grids without a heavy and unrealistic CPU time for an engineering project. We intend to verify the consistency of results obtained within the framework of a standard engineering study requiring a reasonable calculation power. This current work presents the results of these investigations and develops the methodology for predicting cavitation in a pump.

## 2. EXPERIMENTAL INVESTIGATIONS

### 2.1 Test rig and Helico-centrifugal Pump design

A storage tank with a capacity of 15 m<sup>3</sup> is connected to an airdome. This airdome is a smaller tank that can be filled and emptied. A liquid ring vacuum pump is used to control the pressure at the free surface inside this tank. A 200 kW alternate current motor powered by a variable frequency controller is used to drive the tested pump. The rotational speed is measured using an optical sensor connected on a frequency meter (accuracy 0.3%). A motorized regulating valve allows the control of the flow rate. An electromagnetic flowmeter (accuracy 0.5%) located at the pump outlet, at a sufficient distance away from the pump exit, so that the flow is not too disturbed. Pressure levels are measured through transmitters (accuracy 0.3%). They are located at the inlet and outlet sections and give the average tip pressure on four pressure tapping. A temperature probe (accuracy 0.5%) is also used. One should note that the average temperature during the tests is below 28°C.



**Fig. 1 :** Pump geometry

**Fig. 2 :** Runner view

A helico-centrifugal pump is a centrifugal pump, with a mixed flow type impeller. Indeed, the main flow path is nor radial, nor axial but conical. The pump consists of a centrifugal four blade impeller in an axisymmetric volute with a radial outlet [Fig.1 et Fig.2].

## 2.2 General Overview of experimental procedure

The impeller is equipped with a transparent acrylic shroud and the test section is optically accessible by windows in the side of casing for visual inspection of the cavitation [Fig.1]. A stroboscopic light source was used for illumination of the optical observations. At each operating point, a picture is taken at the pressure side and the suction side of the blade. Thanks to the grid drawn on the blade, it is easy to sketch the cavitation gas pocket and its development during the test. The procedure for the experiments is the following: the impeller rotational speed is fixed at 1485 rpm. The flow rate is set to the operating value using the motorized control valve. It varies from 0.85 Q<sub>n</sub> to 1.25 Q<sub>n</sub>. The inlet pressure drop is obtained by the liquid vacuum pump.

A large range of flow rates was investigated around the nominal point of operation in non cavitating and cavitating conditions. For the cavitating cases, a level of static pressure equal to 7 bars prevents from the appearance of vapor. In cavitating conditions, the flow rate is kept constant, and the static pressure is decreased slowly to enhance vapour development in the impeller and reach the performance breakdown.

## 3. NUMERICAL AND PHYSICAL ASPECT

### 3.1 Cavitation modeling

To describe the cavitation process, the fluid flow into the pump has to be considered as a multiphase flow composed of non-condensable gas (g), vapour (v) and liquid (l). The relative quantity of each component can be described by a scalar volume fraction:  $\alpha_g$  for incondensable,  $\alpha_v$  vapour and  $\alpha_l$  liquid with a sum equal to unity. In the current cavitation models, only two phases are considered : the liquid (or pure substance mixture: liquid + non-condensable) and vapour are assumed to be mechanical equilibrium (no interphase slip). They are based on the so-called VOF (Volume of Fluid) model. A source term into the volume-of-fluid equation Eq.(1) is provided by a Rayleigh-Plesset equation governing bubble dynamics. This model assumes a thermal equilibrium, on a zero slip velocity bubble and without bubble interactions. A first order approximation explicitly gives the equation of the rate Eq.(2) et Eq.(3) controlling the vapour generation (vaporization) / destruction (condensation), neglecting the viscous damping, the surface tension and initial bubble acceleration effects. Mass exchange between vapour and liquid (or mixture: Liquid + Non-condensable) is given by the equations below:

$$\frac{\partial}{\partial t}(\rho_l \alpha_l) + \frac{\partial}{\partial x_j}(\rho_l u_j \alpha_l) = \dot{m}_l^c - \dot{m}_l^v \quad (1)$$

with

During vaporization:

$$\dot{m}_l^v = F^v \frac{3\alpha_g \alpha_l \rho_v}{r_0} \sqrt{\frac{2}{3} \max\left(\frac{P_v - P}{\rho_l}, 0\right)} \quad (2)$$

During condensation:

$$\dot{m}_l^c = F^c \frac{3(1 - \alpha_l) \rho_v}{r_0} \sqrt{\frac{2}{3} \max\left(\frac{P - P_v}{\rho_l}, 0\right)} \quad (3)$$

In this model, the bubble pressure or rather phase change threshold pressure is assumed to be equal to the vapour saturation pressure in absence of dissolved gas. This value is evaluated at the temperature of the surrounding liquid. The non-condensable gases with a volume fraction ( $\alpha_g$ ) are assumed to be present as spherical bubbles which provide nucleation sites. The values generally taken for  $\alpha_g$  are:  $5 \cdot 10^{-7}$  [13],  $10^{-5}$  [2]; [3], and  $5 \cdot 10^{-4}$  [27]; [28]; [33]. Extreme values have been tested here. These authors assume an initial radius for the nuclei ( $r_0$ ) equal to  $10^{-6}$ m, this value has been retained. The constants FV and FC are introduced to account for the fact that the vaporization and condensation processes have different times scales. Their values, FV = 0.01 and FC = 50 are derived from numerical testing, using experimental data of the cavitating flow on a two-dimensional hydrofoil [2]; [3]; [10].

The vapour density can be calculated using an ideal gas relation. For a low speed flow, the vapour density can be assumed as a constant value, estimated at the vapour pressure and fluid temperature. In this work, the fluid temperature is also considered constant at a typical value observed during the experiments,  $T=300$  K.

In spite of computing power increase, the Reynolds-averaged Navier-Stokes (so-called RANS) equations are always mainly used for the 3D problems and particularly Eddy Viscosity Models [21]. Eddy Viscosity Model are often used in the numerical study of cavitation phenomena in turbomachines: k- $\epsilon$  standard [4]; [10]; [27]; [28], k- $\epsilon$ -RNG variant [11]; [16]; [17], or k- $\omega$  formulation [12]; [25]. In this study, the k- $\epsilon$  and SST model have been compared for non-cavitating cases. For adverse pressure gradient, the SST model gives better results than the k- $\epsilon$  model. In 3D cases, this model requires too fine a grid which makes it inapplicable on turbomachinery cases. This explains why the one does not observe large differences in the solutions given by both models [6]; [14].

### 3.2 Computational methodology

The commercial packages ANSYS-CFX solve the Reynolds-averaged Navier-Stokes (RANS) equations with a finite-volume/finite-element method [1]. The solution of the velocity-pressure system is based on a fully coupled approach. The implementation of resolution scheme (solver, interpolation scheme, Coriolis effect...) in ANSYS-CFX has been found to be very robust and efficient in predicting swirl flow in turbomachinery [7]; [30].

ANSYS-CFX is a three dimensional unstructured mesh code. However, multiblock structured meshes are used here with the two codes. The meshes are generated with CFX-TurboGrid (V.1.6.03) a specific mesher dedicated to turbomachinery. Multiblock structured mesh is still widely used and preferred by CFD analysts for it is the best suited for turbomachinery applications. Indeed, it allows the best quality mesh in the wheel region while keeping a reasonable number of cells. It is important to note that the so-called CV-FEM method (control volume/finite-element method) remains efficient on hexahedral meshes while the use of tetrahedral meshes tends to degrade its efficiency.

A grid dependency study is first carried out on a non-cavitating flow. Selected final mesh consists for a single blade passage of 220 000 nodes. Specific cell thickness progression laws in the meridian, hub-to-shroud and blade to blade directions are applied to ensure good grid quality: near wall orthogonality is enforced and slightly skewed mesh is observed in the remainder of the domain with a maximum element aspect ratio lower than 1000; cells evolution factor is lower than 1.25 [Fig.3].

The numerical prediction of cavitating flows is a difficult problem and often requires small time steps to control the non-linearity generated by the model. To keep the CPU time reasonable, the model includes only the wheel. The computing domain to predict to cavitating flow consists in a single blade to blade passage. The boundary conditions used are total pressure at the inlet and mass flow at the outlet. The connection between the periodic faces is made by periodic connections.

Experiments results include measures of pressure values at the pump inlet and casing outlet. It is therefore necessary to also measure the global values of the pump itself in order to derive the pressure drop due to the volute. The CFD results on the wheel only can then be compared to the experiments. The prediction of the pump global values has been performed in a non cavitating regime. The whole wheel was meshed (4 x 220 000 nodes). The volute was meshed with ICEM CFD Hexa. The whole pump mesh consists of 1.2 million nodes. The flow through an impeller and the volute is considered in steady-state-regime, in which the impeller is solving in a rotating frame and the volute is solved in the stationary frame. The two frames of reference connect to each other in such a way that they each have a fixed relative position throughout the calculation, with the frame transformation along a sliding interface (Frozen-Rotor interface) [1].

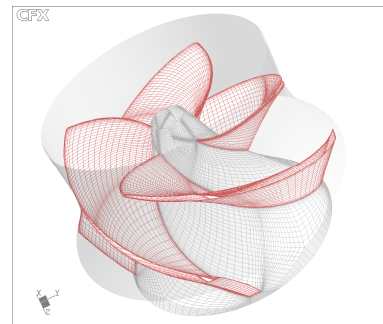


Fig. 3: Mesh visualisation

## 4. Results

### 5.1 Non-cavitating flow

The table [Table 2] compares the results obtained for the three operating modes considered for the {impeller + volute} case. The results for the sole wheel are given in the same table for 0.85Q<sub>n</sub> and Q<sub>n</sub>. The specific energy supplied by the impeller to the flow and the corresponding energy coefficient, are given by:

$$E_t = \frac{\vec{T}_t \cdot \vec{\Omega}}{\rho Q} \text{ and } \psi_t = \frac{E_t}{\Omega^2 R^2} \quad (4)$$

Where  $\vec{\Omega}$  is the angular rotation speed and  $\vec{T}_t$  is a torque determined by the pressure and the viscous forces integrations on the blades and impeller side walls [24]. The energy transferred to the flow, and the corresponding specific energy coefficient (Pressure coefficient), are calculated using the hydraulic energy difference between the low pressure and the high pressure section of the considered element [6]; [24].

$$E = gH \text{ and } \psi = \frac{E}{\Omega^2 R^2} \quad (5)$$

Where H is head of considered element : the wheel alone or the entire pump. The loss can be evaluated by comparing these coefficients. One should observe the important losses caused by the volute. This is due to its special shape that facilitates the visualization of cavitation pockets: the sharp angles are likely to trigger strong local eddies [Fig.4]. The table [Table 2] also points out that the nominal point would correspond to the partial flow 0.85Q<sub>n</sub>. Q<sub>n</sub> which is the point of design corresponds rather to an overload condition. This discrepancy was confirmed during the testing [Fig.5]. Values obtained in experiments and by computation are in excellent agreement.

Model : Wheel + volute					Model:impeller alone		
		0.85Q <sub>n</sub>	Q <sub>n</sub>	1.25Q <sub>n</sub>		0.85Q <sub>n</sub>	Q <sub>n</sub>
Wheel alone	ψ	0.450	0.361	0.213	ψ	0.437	0.356
	ψ <sub>t</sub>	0.491	0.401	0.255	ψ <sub>t</sub>	0.474	0.381
	η <sub>T</sub>	0.915	0.903	0.835	η <sub>T</sub>	0.921	0.92
Pump	ψ	0.353	0.277	0.117			
	η <sub>T</sub>	0.720	0.693	0.457			

Table 2: Non cavitating flow – Performances

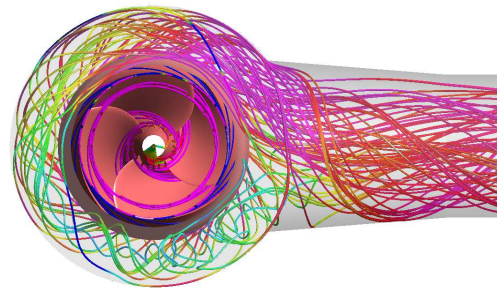


Fig. 4: Structure of the flow in the volute - Free cavitation

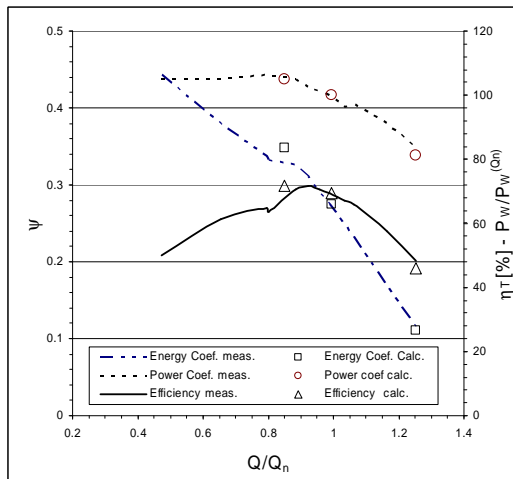


Fig. 5: Cavitation Free - Comparison Experimental results – Numerical Prediction: (Energy Coef.), P<sub>w</sub>/P<sub>w</sub>(Q<sub>n</sub>) (Power Coef.), (Efficiency)

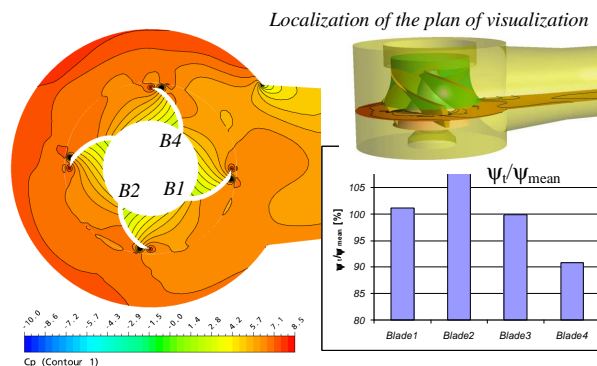


Fig. 6: influence volute on the pressure field and on the torque (ψ<sub>t</sub>) of each blade

The energy transferred through the impeller alone ( $\psi_i$ ) is lower than the energy transferred to the whole model (5%). The ratio on each blade of the specific energy on the average value shows the effect of the volute of the energy transfer mechanism in the pump. The influence remains mostly localized at the blade pressure side at the impeller exit. It has no significant effect on the pressure along the suction side [Fig.6]. This indicates that for number of cavitations beyond the critical values corresponding to the head drop, the influence of the volute does not play a major role in the impeller inception of cavitation, thus legitimizing the fact to consider as a first approach the impeller alone.

## 5.2 Cavitating flow

The specific energy coefficient  $\psi$  Eq.(5) is plotted as a function of the cavitation number  $\sigma$  [Fig.7]. The experimental values are compared on the same graph. The agreement between experimental results and numerical predictions is quite acceptable. But the critical cavitation number ( $\sigma_c$ ) is systematically underestimated by the simulation. The numerical head-drop occurs with lower values of cavitation number and is steeper than the experimental curve. What prevents from differentiating breakdown number ( $\sigma_b$ ) from critical cavitation number ( $\sigma_c$ ). This gap may be due to the facts that the pocket instabilities were not taken into account in a cavitation model. It can also be attributed to the selected values for the empirical

coefficients of vaporization and condensation terms, to the restrictions of the turbulence model, and to the too coarse mesh [28]. Moreover, in this case and at the critical values of  $\sigma$ , the leakage flow was not accounted as the impeller alone was considered. However, the influence of the volute may not be negligible in the phenomena [21].

When the beginning of performance drop occurs, a difference between experimental and numerical results may be observed. At partial flow, the experimental curve starts to drop for a higher cavitation number. This drop is not predicted, and on the contrary, a slight increase in the head is computed. At nominal point, the start of this drop is closer to the value of breakdown cavitation number than for the partial flow case: again, the computational model only predicts an almost sudden drop in the performance. At overload condition, the simulations are in better agreement with the experiments: the drop of the performance curve is preceded by a noticeable increase of the head. However, the slope of the drop is still overestimated.

This inability of the simulation to predict a progressive decrease of the performance (prior to the complete blockage effect) can be explained by a late inception of the cavitation. Now, several simulations have been performed with different values [2]; [11]; [13]; [28]; [33] for the empirical model coefficients such as the constants of vaporization and condensation, the volume fraction of incondensable, nuclei mean radius. they did not show significant differences in the head-drop curves. The introduction of turbulent pressure fluctuations in phase change threshold pressure not improved this behaviour [5]; [34].

The figures [Fig.8a,b,c] show the development of cavitation pockets observed experimentally in the blades and the ones predicted in CFX. The threshold value used for the iso-surface that represents the cavitation pocket was set at  $\alpha_v=0.01$ . The pocket developments near leading edge (surface and position of the cavity closure) are in very good agreement with the experiments.

At flow rate corresponding to  $0.85 Q_n$  [Fig.8a], the predicted shapes compare perfectly well with the ones observed for the pressure values from  $\sigma = 0.8$  to the critical numerical value  $\sigma = 0.12$ . Still, this

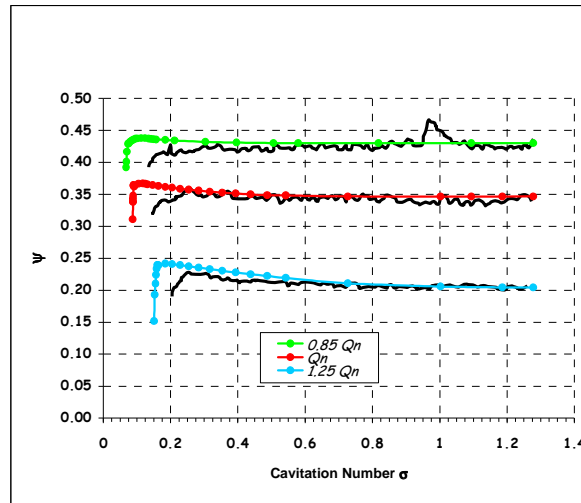
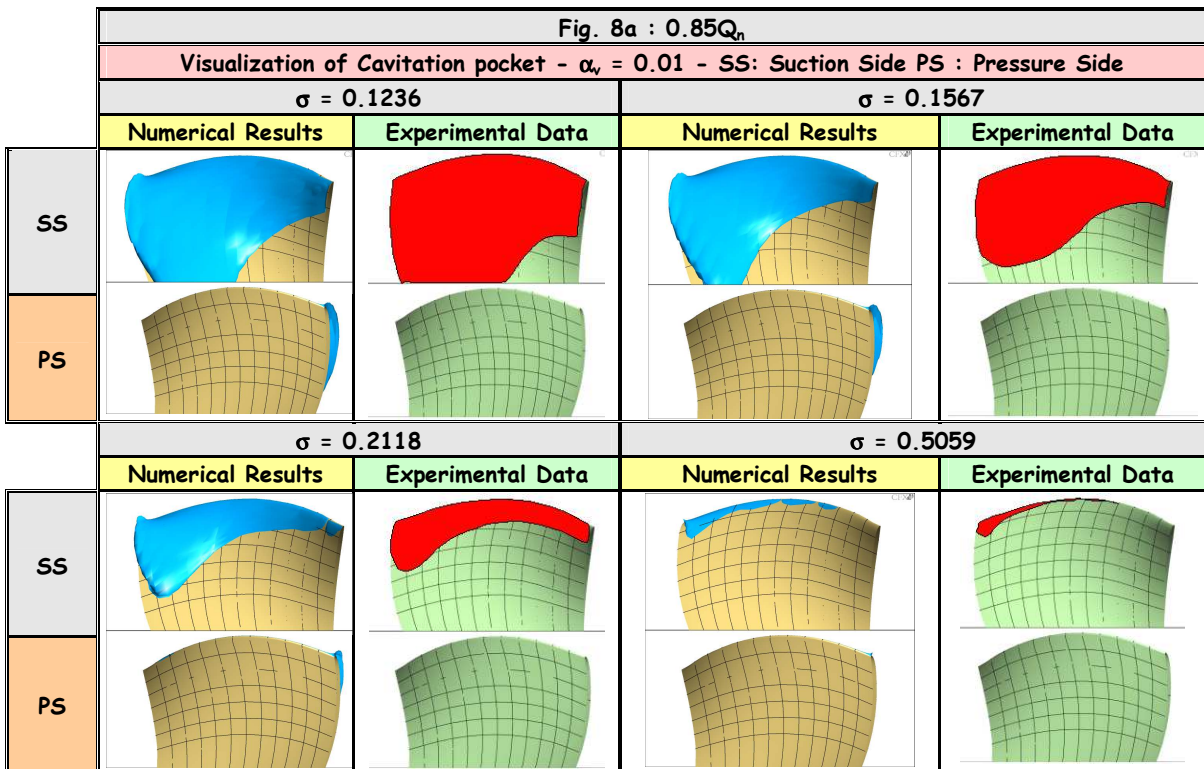
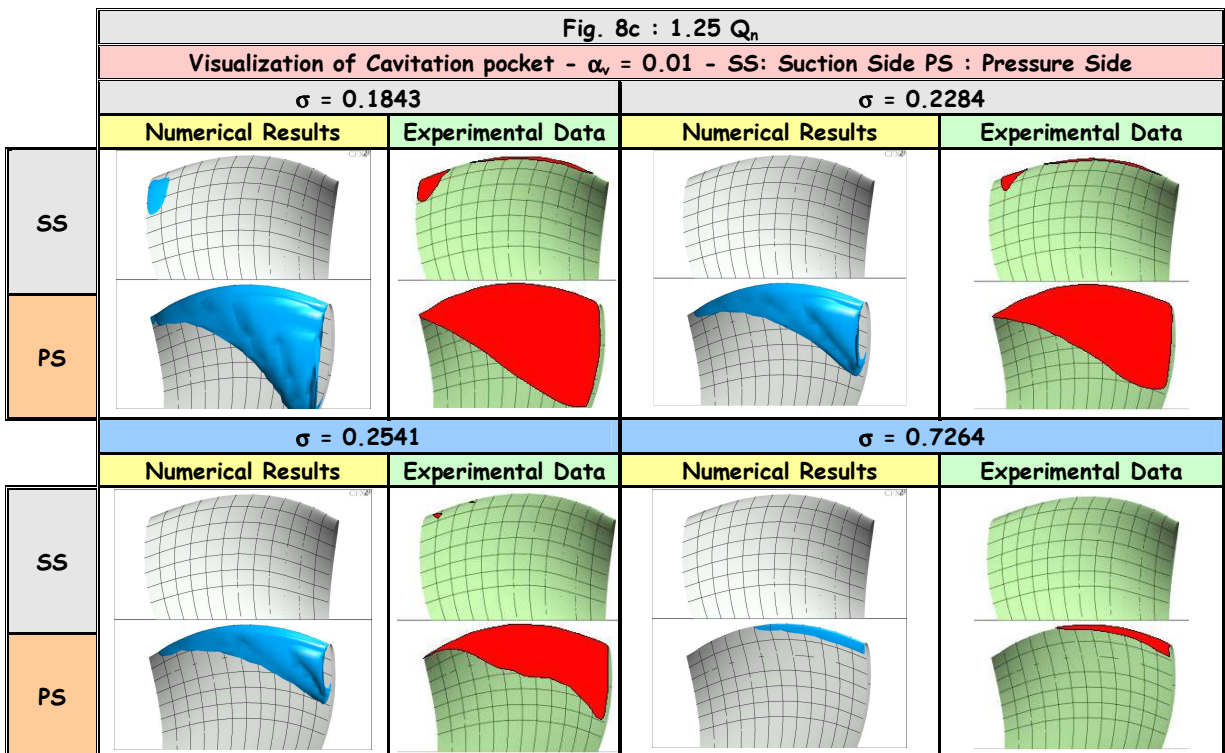
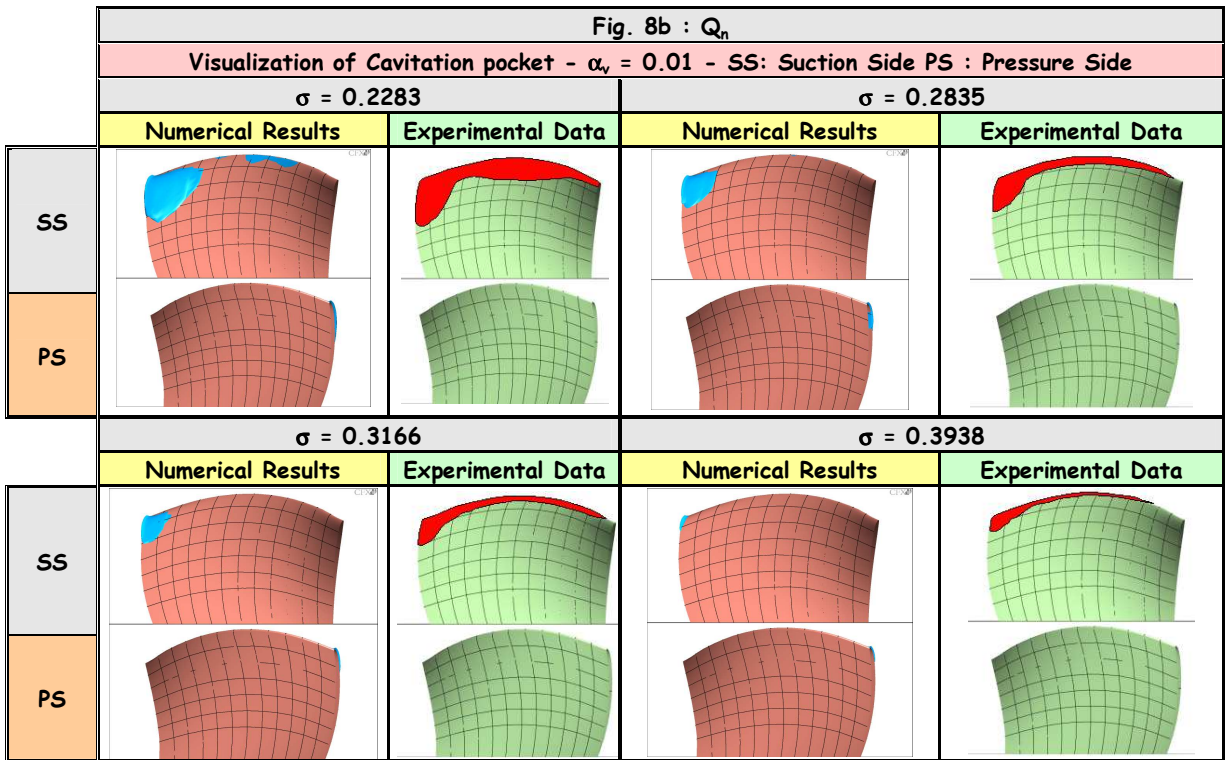


Fig. 7: Head-drop curves in cavitating conditions: comparison of supplied energy coefficients  $\psi$  at  $0.85Q_n$ ,  $Q_n$ ,  $1.25Q_n$

does not help to predict the beginning of the performance drop observed from  $\sigma_{d,measured} = 0.28$  ( $\sigma_{c,measured} = 0.113$ ). The mesh at the leading edge is not fine values of  $\sigma$  larger than 0.8.

At the nominal point [Fig.8b]; the comparison between testing and computation is not as well as the previous case. However, one observes that for values of  $\sigma$  larger than 0.39, an increase of the specific energy received by the fluid is consistent; this effect is most certainly related to the presence of cavitation pocket near the shroud. For values smaller than  $\sigma = 0.23$  ( $\sigma_{d,measured} = 0.23$ ,  $\sigma_{c,measured} = 0.14$ ), this zone generates unstable bubble shedding. This unstable behaviour increases as the cavitation number decreases, leading to unstable detachment of the cavitation pockets along the line of closing. These phenomena can trigger off performance drop. This is obviously not captured by our steady state simulations. At overload condition [Fig.8c], the shapes and positions of pockets observed in experiments are quite correctly predicted for values of  $\sigma$  lower than 0.26 and approaching the computational critical value of  $\sigma = 0.16$ . When flowrate value is above the nominal point, these pockets are developing at the pressure side of blade. However, as for the partial flow case, this good agreement does not allow to predict the decrease of the performance that appears at  $\sigma_d = 0.23$ ,  $\sigma_c = 0.2$ . Concerning the two off-design conditions, the pockets have a stable behaviour. Some transient phenomena can be noticed but remain localized to the region of closure, which does not vary much with the extension of the pocket. This leads us to think that unlike for the nominal point, the performance drop is not caused by the unstable behaviour of the pockets but perhaps is due to an inadequate description of the boundary layer downstream the cavitation zone. For values of  $\sigma$  larger than 0.26, the increase of the energy received by the fluid is correctly reproduced by the simulation. One can notice though, that for values above 0.45, a slight difference appears in the extensions of the pockets; these differences can be related to the spatial definition of this zone.





The curves in figure [Fig.9] give, for the 3 operating conditions, the evolution of the specific energy supplied by the impeller and the one of the specific energy transferred to the flow. These coefficients are divided by the ones obtained from the non-cavitating simulation. The coefficients  $\sigma_d$  are also reported on the curves: they correspond to the start of performance drop. In experiments, cavitation appears rapidly through stable pockets at quite high cavitation numbers:  $\sigma = 1.1$  at  $0.85Q_n$ ,  $\sigma_c = 0.7$  at  $Q_n$ ,  $\sigma_c = 1.2$  at  $1.25Q_n$ .

When the cavity closure moves away from the blade edge, the specific energy coefficient increases from the following values:  $\sigma = 0.4$  at  $0.85Q_n$ ,  $\sigma = 0.5$  at  $Q_n$ ,  $\sigma = 1.25$  at  $1.25Q_n$ . The decrease of head, observed in experiments indicates that transferred energy decreases faster than the supplied energy.

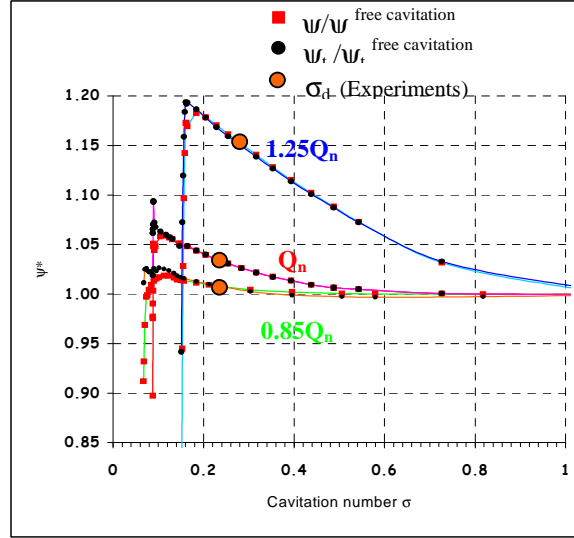


Fig. 9: Head-drop curves in cavitating conditions: comparison of supplied  $\psi$  and transferred energy coefficients  $\psi_i$ , at  $0.85Q_n$ ,

In order to explain the increase of the head for the lowest cavitation number, the  $\beta$  coefficient can be compared between cavitation and cavitation-free conditions. The  $\beta$  coefficient is defined as the angle between absolute velocity and meridional velocity [Fig.10].

The mean meridional velocity is given by the following equation :

$$\overline{Cm}_{SPAN} = \frac{1}{r_{SPAN} \Delta\theta} \int Cm \cdot r_{SPAN} d\theta \quad (6)$$

So, the  $\beta$  angle is computed as :

$$\beta_{SPAN} = \text{Arc sin} \left( \frac{\overline{Cm}_{SPAN}}{\overline{Cu}_{SPAN}} \right) \quad (7)$$

The cavitation development entails the increase of  $\beta$  angle at the leading edge for the lower cavitation number. By integrating the  $\beta$  angle span by span, the mean  $\beta$  is plotted from hub to shroud [Fig.11]. The 15% head curve increasing observed for  $1.25Q_n$  can be explained by the offset of the mean  $\beta$  curve between two configurations  $\sigma = 1$  and  $\sigma = 0.254$ .

The decrease of head, observed in experiments indicates that transferred energy decreases faster than supplied energy [Fig. 9]. Hydrodynamic losses due to cavitation development are dramatically underestimated by simulation. It may be explained by a too coarse grid of the cavitation area generating a weak feedback on the deformation of the flow. It is perhaps necessary to refine strongly the mesh. The increasing of the node number allows to improve the simulation of the deformation of the flow near to the wall what could let taking into account of the maximum tensile stress term in phase threshold pressure [5].

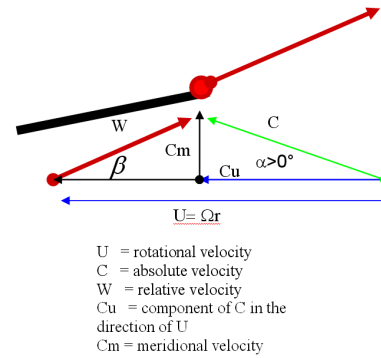


Fig. 10: Geometric representation of beta angle

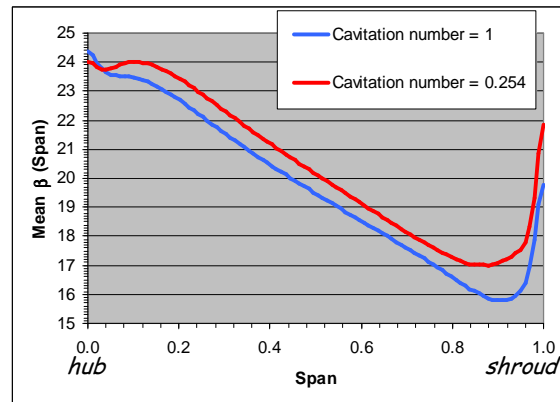


Fig. 11: Evolution of mean  $\beta$  between hub and shroud ( $1.25 Q_n$ )

## 5. CONCLUSION

CFD Simulation of the flows in the hydraulic turbo-machineries always obliges to find a compromise between smoothness of grid and precision necessary to correctly predict the included phenomena. For non-cavitating flow, the mesh grids usually used (200 000 to 300.000 nodes/passage) make it possible to obtain reliable results in particular to evaluate the performances of the pumps, if we don't move away too much from the nominal point. Indeed in this case, more complex flow structures can appear requiring to refine the grid and to extend the domain of calculation which will not be limited any more at only one passage but risk to extend to the whole pump, giving time consuming calculations. Moreover, to benefit from models of turbulence able to describe the boundary layer, the density of nodes will be likely to be high close to the walls. In the case of the simulation of cavitating flow, times calculations will be amplified, the more the non-linear behaviour of the model often obliges to under-relax the solver, in particular when one approaches the critical points.

The use of the cavitation model based on the VOF approach, of the first order approximation of the Rayleigh-Plesset equation, of a domain of calculation limited to only one passage and of a number of elements of discretization which ensures for a non cavitating flow an acceptable compromise between precision and CPU time (220 000 nodes), makes it possible to predict correct behaviour of the cavitating flow in the helico-centrifugal pump.

For the three operating conditions considered, simulations predict extents of cavitation pockets in conformity with those observed in experiments: position, size. The numerical results confirm that the cavitation zones located downstream from the leading edge and close to the shroud become unstable when the pressure of inlet corresponds to the experimental value where the head starts to decrease. The precision of evaluation of the convective terms plays a major part in the prediction of the pockets. The strategy used in ANSYS-CFX resting on Numerical Advection Correction respecting a multidimensional criterion of monotony seems effective. The more so as this gain of precision can become capital during non stationary simulations, in condition however of reformulating the evaluation of turbulent viscosity and of the threshold pressure of the cavitation model. Because, in the contrary, we can artificially stabilize the pockets of cavitation. The use of grids based on hexahedral elements remains preferable. In the same order, the expansions and the deformations of mesh must remain moderate. Because in the contrary case, the evaluation of the gradients of the node center will be able to degrade the gain of precision brought by the corrective term. And this degradation will be all the more significant on a skewed element if the criterion of monotony is applied to all the contributions of the corrective term of the scheme.

The calculations make it possible to reproduce the extent of the pockets and the increase head observed in experiments, during the reduction of the inlet pressure. This phenomenon corresponds to a modification of the pressure distribution downstream from the cavitation pockets. However, they do not succeed in predicting the appearance of the measured head-drop. Calculations continue to predict an increase in head, until the quasi simultaneous fall of head and torque. This phenomenon of quasi breakdown appears when the cavitating zone enlarges and reaches an opposite side of the adjacent blade. From the impeller geometry, this area is near of the outlet of the passage. One reason not making possible to predict the head-drop correctly, can be due to a pressure level too much low compared to the tests to initiate such a phenomenon.

Before prospecting towards more advanced models: physical model take in account the water quality (full cavitation model [34]), leakage flow and influence of the casing, we must first check that a better description of the boundary layer in this zone: meshing and model, can correct this delay. The instationary behaviour observed at the nominal flow rate will have to be also taken into account. In a general way, the refinement of the mesh will lead towards numerical difficulties obliging to simulate in a non stationary mode the flow in the complete impeller!

## 6. ACKNOWLEDGEMENTS

We would like to thank Guido Doebener, ANSYS inc., Otterfing, Germany for his collaboration during the project.

## 7. REFERENCES

- [1] ANSYS-CFX, Release 10.0, Computational Fluid Dynamics Software, Solver Guide, 2005.
- [2] Ait Bouziad y, Guennmoun F., Farhat M., Avellan F., Numerical Simulation of Leading Edge Cavitation, Proceedings of FEDSM'03 4th ASME-JSME Joint Fluids Engineering Conference, July 6-11, Honolulu, Hawaii, USA, 2003.
- [3] Ait Bouziad y, Farhat M., Guennmoun F., Kueny J.L., Avellan F., Physical Modelling and Simulation of Leading Edge Cavitation, Application to an Industrial Inducer, Fith International Symposium on Cavitation, November 1-4, Osaka, Japan, 2003.
- [4] Ait Bouziad Y., Farhat M., Kueny J.L., Avellan F., Miyagama K., Experimental and numerical cavitation flow analysis of an industrial inducer. 22nd IAHR Symposium on Hydraulic Machinery and Systems, June 29 – July 22, Stockholm, Sweden, 2004
- [5] Ait Bouziad Y., Physical modelling of leading edge cavitation: Computational methodologies and application to hydraulic machinery. PhD thesis, Ecole Polytechnique Fédérale de Lausanne, 2006 (N°3353)
- [6] Asuaje M, Bakir F., Kouidri S., Kenyery F., Rey R., Numerical Modelization of the Flow in Centrifugal Pump: Volute Influence in Velocity and Pressure Fields, International Journal of Rotating Machinery 3:244-255, 2005.
- [7] Athavale M.M, Li H.Y., Jiang Y., Singal A. K., Application of the full cavitation model to pumps and Inducers, International Journal of Rotating Machinery, 8: 45-56, 2002.
- [8] Bache G., Thomas M., Validation an Efficient and Accurate Turbomachinery CDX Analysis Procedure, in 28th Aerospace Sciences Meetings, AIAA Paper 98-681, January 8-11, 1990.
- [9] Bachert R., Ludwig G., Stoffel B., Frobenius M., Schilling R., Three-Dimensional Unsteady Cavitation Effects on a Single Hydrofoil and in a Radial Pump-Measurements and Numerical Simulations, Fith international Symposium on Cavitation, November 1-4, Osaka, 2003.
- [10] Bakir F., Mejeri I., Kouidri S., Rey R., Hub Shape Effects under Cavitation on the Induceurs Performance, Fith International Symposium on Cavitation, November 1-4, Osaka, 2003.
- [11] Bakir F., Rey R., Gerber A.G., Belramri T., Hutchinson B., Numerical and Experimental Investigations of the Cavitating Behavior of an Inducer, The International Journal of Rotating Machinery, Volume 10, Number 1 / Jan-Feb, 2004.
- [12] Basuki W., Schnerr G.H., Yuan W., Single-Phase and Modified Turbulence Models for Simulation of Unsteady Cavitating Flows, Wissenschaftliche Berichte FZKA, 6759:F.14-F.29, 2003.
- [13] Catelan F.X., Ouabi A., Cavitation dans une roue centrifuge (Pompe Volute béton) à l'aide du logiciel TASC-Flow 2.12 et comparaison avec les résultats expérimentaux, Proceedings de la 164ème session du Comité Scientifique et Technique SHF, Colloque d'Hydrotechnique, 7 avril, Chatou, France, 2005.
- [14] Combes J.F, Boyer A., Gros L, Pierrat D, Pintran G, Chantrel P, Experimental and numerical investigations of the radial Trust in a Centrifugal Pump, ISROMAC12-2008-20074, February 17-22, Hawaii, 2008.
- [15] Combes, J.F., Archer, A., Etude de l'érosion de cavitation dans la pompe SHF, Proceedings de la 164ème session du Comité Scientifique et Technique SHF, Colloque d'Hydrotechnique, 21-22 Novembre, Chatou, France, 2000.

- [16] Coutier-Delgosha O., Astolfi J.A., Numerical Prediction of The Cavitating Flow on a Two-Dimensional Symmetrical Hydrofoil with a Single Fluid Model, Fith International Symposium on Cavitation, November 1-4, Osaka, Japan, 2003.
- [17] Coutier-Delgosha O., Fortes-Patella R., Hofmann M., Stoffel B., Experimental and Numerical Studies in a Centrifugal Pump With Two-Dimensional Curved Blades in Cavitating Condition, *Journal of Fluids Engineering*, 125:970-978, 2003
- [18] Coutier-Delgosha O., Morel P., Fortes-Patella R., Reboud JL., Numerical Simulation of Turbopump Inducer Cavitating Behavior, *Int. Journal of Rotating Machinery*, 2:135-142, 2005.
- [19] Friedrichs J., Kosyna G., Unsteady PIV Flow Field Analysis of a Centrifugal Pump Impeller Under Rotating Cavitation, Fith International Symposium on Cavitation, November 1-4, Osaka, Japan, 2003.
- [20] Hanjalic K., Will RANS Survive LES? A View of Perspectives, *Journal of Fluids Engineering*, 127:831-839, 2005.
- [21] Hirschi R., Dupont Ph., Avellan F., Favre J.N., Guelich J.N., Handloser W., Parkinson E., Centrifugal Pump Performance Drop due to Leading Edge Cavitation: Numerical Predictions compared with Model Tests, *Journal of Fluids Engineering*, 120: 705-711, 1998.
- [22] Hosangadi A., Ahuja V., A New unsteady Model for Dense Cloud Cavitation in Cryogenic Fluids, *Proceedings of FEDSM2005*, June 19-23, Houston, TX, USA, 2005.
- [23] Hoffman M., Stoffel B., Coutier-Delgosha O., Fortes-Patella R., Reboud JL., Experimental and Numerical Studies on a Centrifugal Pump with 2D-Curved Blades in Cavitating Condition, *Fourth International Symposium on Cavitation*, June 20-23-4, Pasadena, California, USA, 2001.
- [24] Hoffman M., Stoffel B., Friedrichs J., Kosyna G., Similarities and Geometrical Effects on Rotating Cavitation in Two Scaled Centrifugal Pumps, *Fourth International Symposium on Cavitation*, June 20-23-4, Pasadena, California, USA, 2001.
- [25] Kawamura T., Sakoda M., Comparison of Bubble and Sheet Cavitation Models for Simulation of Cavitating Flow Over A Hydrofoil, *Fith International Symposium on Cavitation*, November 1-4, Osaka, Japan, 2003.
- [26] Luo X., Nishi M., Yoshida K., Dohzono H., Miura K., Cavitation Performance of a Centrifugal Impeller Suitable for a Mini Turbo-Pump, *Fith International Symposium on Cavitation*, November 1-4, Osaka, Japan, 2003.
- [27] Mejeri I., Bakir F., Rey R., Experimental and Numerical Analysis of Unsteady Cavitation Instabilities in an Axial Inducer, *Sixth International Symposium on Cavitation*, September 11-15, Wageningen, Netherlands, 2006
- [28] Mejeri I., Bakir F., Rey R., Comparaison of Computational Results Obtained From a Homogeneous Cavitation Model With Experimental Investigations of Three Inducers, *Journal of Fluids Engineering*, 128:1308-1323, 2006
- [29] Pierrat D., Gros L., Pintrand G., Le Fur B., Gyomlai P., Experimental and numerical investigations of leading edge cavitation in helico-centrifugal pump, *ISROMAC12-2008-20074*, February 17-22, Hawaii, 2008.
- [30] Pouffary B., Fortes-Patella R., Reboud JL., Numerical Simulation of Cavitating Flow around a 2D Hydrofoil: A barotropic Approach, *Fith International Symposium on Cavitation*, November 1-4, Osaka, Japan, 2003.
- [31] Raw M., Robustness of Coupled Algebraic Multigrid for the Navier-Stokes Equations, *AIAA 96-0297*, 1996.

- [32] Saito Y., Nakamori I., Ikohagi T., Numerical Analysis of Unsteady Vaporous Cavitating Flow around Hydrofoil, Fifth International Symposium on Cavitation, November 1-4, Osaka, Japan, 2003.
- [33] Scheuerer G., Development and Validation of a Cavitation Model in CFX5, Proceedings de la 164ème session du Comité Scientifique et Technique SHF, Colloque d'Hydrotechnique, 7 avril, Chatou, France, 2005.
- [34] Singhal A.K., Athavale M.M., Yang H.Q., Recent advances (Ventilated Cavitation) with the Full Cavitation Model, Eccomas 2004, Jyväskylä, July 24-28, 2004.

## 8. NOMENCLATURE

$F^C, F^V$	[-]	Cavitation modelling parameter	$\alpha$	[-]	Volume fraction
$g$	[m/s <sup>2</sup> ]	Acceleration due to gravity	$\Delta P_{Loss}$	[Pa]	Loss $\Delta P_{Loss} = P_{total\ relatif, in} - P_{total\ relatif, out}$
$H$	[m]	Head $H = \frac{\Delta P_t}{\rho g}$	$\Delta P_{total}$	[Pa]	Total pressure variation $\Delta P_{total} = P_{total, in} - P_{total, out}$
$\dot{m}_i^C$	[kg/s]	Mass transfer between vapor and liquid, condensation process	$\eta_P$	[-]	Efficiency based on pressure $\eta_P = \frac{\Delta P_{total}}{\Delta P_{total} - \Delta P_{Loss}}$
$\dot{m}_i^V$	[kg/s]	Mass transfer between vapor and liquid, evaporation process	$\eta_T$	[-]	Efficiency based on torque $\eta_T = \frac{\Delta P_{total} Q}{\bar{T} \cdot \Omega}$
$NPSH$	[m]	Net Positive Suction Head $NPSH = \frac{P_{in} - P_{sat}}{1/2 \rho U_{in}^2} + \frac{u_{in}^2}{2g}$	$\rho$	[kg/m <sup>3</sup> ]	Density of mixture
$P$	[Pa]	Local static pressure	$\sigma$	[-]	Cavitation number $\sigma = \frac{g NPSH}{\Omega^2 R^2}$
$P_V$	[Pa]	Vapour saturation pressure	$\sigma_b$	[-]	Breakdown cavitation number corresponding to a fall of the total pressure
$P_w$	[kW]	Power	$\sigma_c$	[-]	Critical cavitation number corresponding to a drop of 3% of the total pressure variation
$Q$	[m <sup>3</sup> /s]	Flow rate	$\sigma_d$	[-]	Cavitation number corresponding to the appearance of the decrease of the total pressure
$Q_n$	[m <sup>3</sup> /s]	Nominal Flow rate	$\Omega$	[rad/s]	Angular velocity
$R$	[m]	Wheel radius	$\Psi$	[-]	Specific energy transferred to the flow $\Psi = \frac{gH}{\Omega^2 R^2}$
$r_0$	[m]	Initial radius for nuclei	$\Psi_t$	[-]	Specific energy supplied by the whell $\Psi_t = \frac{\bar{T}_t \cdot \bar{\Omega}}{\rho Q \Omega^2 R^2}$
			$\bar{T}$	[N.m]	Torque determined by the pressure and the viscous forces integration on the blades and impeller side walls

### Subscripts

$g$	Non-condensable gas
$i, j$	Cartesian tensor indices
$in, out$	Inlet, outlet boundaries
$l$	Liquid phase
$v$	Vapor phase